



**HAL**  
open science

## Global Chemistry Simulations in the AMMA Multimodel Intercomparison Project

Jason Edward Williams, Rinus Scheele, Peter van Velthoven, Idir Bouarar,  
Kathy S. Law, Béatrice Josse, Vincent-Henri Peuch, Xin Yang, John Pyle,  
Valérie Thouret, et al.

► **To cite this version:**

Jason Edward Williams, Rinus Scheele, Peter van Velthoven, Idir Bouarar, Kathy S. Law, et al..  
Global Chemistry Simulations in the AMMA Multimodel Intercomparison Project. *Bulletin of the  
American Meteorological Society*, 2010, 91 (5), pp.611-624. 10.1175/2009bams2818.1 . hal-00489503

**HAL Id: hal-00489503**

**<https://hal.science/hal-00489503>**

Submitted on 8 Dec 2020

**HAL** is a multi-disciplinary open access archive for the deposit and dissemination of scientific research documents, whether they are published or not. The documents may come from teaching and research institutions in France or abroad, or from public or private research centers.

L'archive ouverte pluridisciplinaire **HAL**, est destinée au dépôt et à la diffusion de documents scientifiques de niveau recherche, publiés ou non, émanant des établissements d'enseignement et de recherche français ou étrangers, des laboratoires publics ou privés.

# GLOBAL CHEMISTRY SIMULATIONS IN THE AMMA MULTIMODEL INTERCOMPARISON PROJECT

BY JASON EDWARD WILLIAMS, RINUS SCHEELE, PETER VAN VELTHOVEN, IDIR BOUARAR, KATHY LAW, BÉATRICE JOSSE, VINCENT-HENRI PEUCH, XIN YANG, JOHN PYLE, VALÉRIE THOURET, BRICE BARRET, CATHY LIOUSSE, FRÉDÉRIC HOURDIN, SOPHIE SZOPA, AND ANNE COZIC

Comparing the performance of a set of global chemistry-transport models for the West African region highlights the diverse behavior exhibited for convective uplift, advective mixing, and the composition of the tropical troposphere.

The composition of the troposphere over West Africa is influenced by a range of emission sources, including those from anthropogenic activity (e.g., biofuel and fossil fuel consumption), biogenic activity (e.g., from soil), lightning activity, biomass burning activity related to agricultural practices, and stratosphere-troposphere exchange (STE; see, e.g., Sauvage et al. 2007b; Ancellet et al. 2009). It has also been shown that the long-range transport of chemical precursors from, for example, Europe can have a significant effect on the atmosphere over northern Africa (Duncan et al. 2008). The incidence of strong UV radiation in the tropics results in a highly active chemical regime, which determines the atmospheric lifetime of many trace gas species such as CO. To account for all these processes typically requires the use of large-scale global chemistry-transport models (CTMs) including chemical production and loss, wet/dry deposition, emissions, and subsequent mixing of chemical trace species.

The interannual variability of the intensity of biomass burning events, in tandem with the seasonality associated with such burning periods, also

introduces a significant degree of uncertainty with respect to the total global emissions that are subsequently released from such fires for each particular year (van der Werf et al. 2006). To be able to reduce such uncertainty, a variety of satellite data is currently being utilized to produce comprehensive datasets of emission fluxes for a whole range of chemical species. The three dominant datasets currently available are Global Fire Emissions Database version 2 (GFEDv2; van der Werf et al. 2006), GLOBSCAR (Simon et al. 2004), and Global Burnt Area (GBA; Michel et al. 2005). These different satellite products adopt various methodologies that often couple observational data taken from different satellite instruments to some type of regional model, resulting in a range of emission estimates (e.g., Ito and Penner 2005; Bian et al. 2007). For instance, when considering globally integrated emissions, Africa is consistently the most dominant source region for all of the emission datasets (Jain 2007).

Once released, the strong convective transport that occurs over equatorial Africa results in efficient vertical mixing of emissions that are released near

the ground. Moreover, differences in the dynamics and circulation that occur between the Earth's hemispheres during Africa's dry and wet seasons also have the potential to introduce effects for the regional composition of the troposphere. For instance, using a mesoscale model, Sauvage et al. (2007a) have found that in the NH dry season, the African Easterly Jet (AEJ) allows efficient transport of biomass burning emissions released in central Africa to reach the western coast as detected by Measurement of Ozone and Water Vapor by Airbus In-Service Aircraft (MOZAIC) flight data taken in Lagos (6.2°N, 3.3°E). In contrast, during the wet season, emissions that originate from central and southern Africa tend to dominate. Moreover, there is also regional (horizontal) transport of air masses during the winter to equatorial Africa, most notably by the Harmattan and the AEJ, which inhibits vertical mixing during this season (Sauvage et al. 2005). Therefore, any chemical model chosen to investigate the effect that regional emissions have on atmospheric composition over Africa must have the ability to account for the long-range transport of chemical precursors, aerosols, and long-lived trace gases both into and out of the region of interest.

As part of the African Monsoon Multidisciplinary Analysis Multimodel Intercomparison Project (AMMA-MIP; Hourdin et al. 2010), we have performed model simulations for the year 2006, with a focus on Africa. We concentrate on 2006 to exploit the wealth of measurement data taken during an in-

tensive measurement campaign that was performed during July–August of that year (Reeves et al. 2010). For this purpose, we define a set of passive tracer species for the different latitudinal “zones” in Africa to investigate the differences introduced by the various convective transport mechanisms, model resolutions, and meteorology adopted in a set of state-of-the-art global chemistry-transport models. The analysis is conducted using 2D cross sections averaged between ~3°W and 6°E for the latitudes 20°S–40°N (referred to as the 2D transect), which is similar to that used by the global circulation models that are involved in AMMA-MIP (Hourdin et al. 2010). For the chemically active simulations, we use the recent emission estimates that have been derived using the L3JRCv2 burnt area product for the year 2006 and assembled as part of the AMMA project (Lioussé et al. 2004, 2010). These estimates are based on the Global Burnt Area product derived from the SPOT-VEGETATION data (Michel et al. 2005). This dataset provides an alternative to the commonly used GFEDv2 emission datasets derived using the burnt area measurements from the Moderate Resolution Imaging Spectroradiometer (MODIS; Giglio et al. 2006) in conjunction with the Carnegie–Ames–Stanford approach (CASA) biogeochemical model. This is the first time that this version of the L3JRCv2 emission dataset for trace gases has been coupled to such large-scale CTMs.

## DESCRIPTION OF THE PARTICIPATING MODELS.

In total, four different CTMs were involved in this intercomparison exercise, with these being the Laboratoire de Météorologie Dynamique general circulation model and the Interaction with Chemistry and Aerosols (LMDz-INCA; Folberth et al. 2006) model, Météo-France Chemistry and Transport Model (MOCAGE; Teysseïre et al. 2007), Tracer Model version 4 (TM4; Williams et al. 2009), and parallel-Tropospheric Off-Line Model of Chemistry and Transport (p-TOMCAT; Yang et al. 2005). Each model uses a different combination of parameterizations for the description of convective transport, advection, and diffusivity. Here, we provide a brief outline of the main differences.

Both TM4 and p-TOMCAT are driven by 6-hourly European Centre for Medium-Range Weather Forecasts (ECMWF) meteorological data, whereas MOCAGE is driven with the Météo-France Action de Recherche Petite Echelle Grande Echelle (ARPEGE)-Tropiques analysis and LMDz-INCA uses meteorological data from the LMDz general circulation model (GCM), where winds are relaxed (nudged) toward ECMWF fields. For convective mixing, two

**AFFILIATIONS:** WILLIAMS, SCHEELE, AND VAN VELTHOVEN—KNMI, De Bilt, Netherlands; BOUARAR AND LAW—LATMOS, IPSL, Université Pierre et Marie Curie, Paris, France; JOSSE AND PEUCH—CNRM-GAME, Météo-France/CNRS, Toulouse, France; YANG AND PYLE—Centre for Atmospheric Science, and Department of Chemistry, University of Cambridge, Cambridge, United Kingdom; THOURET, BARRET, AND LIOUSSE—Laboratoire d'Aéronomie, University de Toulouse, Toulouse, France; HOURDIN—Laboratoire de Météorologie et Dynamique, CNRS, IPSL, Université Pierre et Marie Curie, Paris, France; SZOPA AND COZIC—Laboratoire des Sciences du Climat et de l'Environnement/IPSL, CEA, CNRS, and UVSQ, L'Orme des Merisiers, Gif-sur-Yvette, France

**CORRESPONDING AUTHOR:** Jason Edward Williams, KNMI, P.O. Box 201, 3730 AE De Bilt, Netherlands  
E-mail: williams@knmi.nl

*The abstract for this article can be found in this issue, following the table of contents.*

DOI:10.1175/2009BAMS2818.1

In final form 13 October 2009

©2010 American Meteorological Society

of the models (TM4 and p-TOMCAT) adopt the Tiedtke (1989) scheme, which is adopted in many large-scale CTMs. The MOCAGE model adopts the parameterization of Bechtold et al. (2001), which has been compared against that of Tiedtke (1989) and shown to be more efficient in transporting air out of the free troposphere (Josse et al. 2004). The LMDz-INCA model uses the scheme of Emanuel (1991), where comparisons against the Tiedtke scheme indicate that stronger convective transport occurs for the Emanuel scheme (e.g., Barret et al. 2010). For advective mixing the approaches range from the relatively simple first-order “slopes” scheme (Russell and Learner 1981; TM4), a semi-Lagrangian scheme (Williamson and Rasch 1989; MOCAGE) to the more computationally expensive second-order moment schemes [LMDz-INCA (Van Leer 1977) and p-TOMCAT (Prather 1986)], where the use of more sophisticated schemes has been shown to limit diffusivity in the upper troposphere (e.g., Bönisch et al. 2008). Moreover, the horizontal resolution of the models over Africa varies between  $0.5^\circ \times 0.5^\circ$  (MOCAGE) and  $2.5^\circ \times 3.75^\circ$  (LMDz-INCA), which introduces differences in the performance of the various physical parameterizations used in each model and the emission fluxes resulting from variations in temporal variability. For the chemistry component,

TM4 contains a tropospheric scheme and constrains the overhead stratospheric ozone column with values taken from the Ozone Monitoring Instrument (OMI) imposed on the climatology of Fortuin and Kelder (1998), p-TOMCAT contains tropospheric chemistry including halogen species and constrains both  $O_3$  and  $NO_x$  (a composite of  $NO$  and  $NO_2$ ) at the model top with zonal means from Law and Nisbet (1996), LMDz-INCA uses values taken from a climatological mean, and MOCAGE simulates its own stratospheric ozone fields by including the necessary chemical processes. A further difference concerns the choice of chemical reaction data adopted for calculating the rate constants of reactive gases, which can lead to differences of  $\pm 10\%$ . For the gas phase photolysis rates, different parameterizations are employed: TM4 uses the approach of Landgraf and Crutzen (1998) modified according the Krol and van Weele (1997), p-TOMCAT uses the approach of Law and Pyle (1993), and MOCAGE and LMDz-INCA use the approach of Madronich and Flocke (1998). All models constrain methane at the surface using a latitudinal-dependent field, which adopts time-dependant values to accommodate yearly increases in the global values. Table 1 outlines the main differences between both the transport and chemistry components used in each model.

**TABLE 1. An overview of the model resolutions, transport parameterizations, and chemical schemes implemented in the global CTMs participating in the AMMA-MIP intercomparison. The MOCAGE model uses a “zoomed” region over Africa.**

Model	Horizontal resolution	Vertical levels	Transport parameterizations	Model top (hPa)	Chemical mechanism
LMDz-INCA	$2.5^\circ \times 3.75^\circ$	19	Van Leer (1977) Emanuel (1991) Hourdin et al. (2006)	3	INCA <sup>a</sup>
MOCAGE	$2.0^\circ \times 2.0^\circ$ ( $0.5^\circ \times 0.5^\circ$ Africa)	47	Williamson and Rasch (1989) Bechtold et al. (2001) Louis (1979)	5	RACM <sup>b</sup> and REPROBUS <sup>c</sup>
TM4	$3^\circ \times 2^\circ$	34	Russell and Lerner (1981) Tiedtke (1989) Holtslag and Boville (1993) Louis (1979)	10	Modified CBM4 <sup>d</sup>
p-TOMCAT	$2.8^\circ \times 2.8^\circ$	31	Prather (1986) Tiedtke (1989) Rasch and Williamson (1990) Wang et al. (1999)	10	ASAD <sup>e</sup>

<sup>a</sup> Further details can be found in Folberth et al. (2006).

<sup>b</sup> Further details can be found in Stockwell et al. (1997).

<sup>c</sup> Further details can be found in Lefèvre et al. (1994).

<sup>d</sup> Further details can be found in Houweling et al. (1998).

<sup>e</sup> Further details can be found in Carver et al. (1997).

For this experiment, we adopt the global emission datasets defined within the European Union (EU) Global and regional Earth-system Monitoring using Satellite and in-situ data (GEMS) project (<http://gems.ecmwf.int>). These are based on a hybrid assembled from the Reanalysis of the Tropospheric Chemical Composition over the Past 40 Years (RETRO) anthropogenic (<http://retro.enes.org>) and GFEDv2 biomass burning (van der Werf et al. 2006) emission datasets, which are both readily available. For Africa, which is defined as the region between 40°S–30°N and 20°W–40°E, we apply the recently developed L3JRCv2 biomass burning and biofuel database (Lioussé et al. 2004; 2010). Comparing the monthly emission fluxes for trace gases such as CO and NO<sub>x</sub> reveals that the L3JRCv2 dataset emits significantly higher quantities of these gases from biomass burning during the season June–August (JJA) compared to the GFEDv2 dataset. For instance, the total emission flux for CO in this region during JJA increases from ~63 to ~165 Tg CO (not shown). Hence, the impact on the composition of the troposphere is potentially large over Africa.

**DESCRIPTION OF THE PASSIVE TRACER REGIONS.** To highlight the differences in the performance of the various combinations of parameterizations adopted for the description of convective and advective transport and mixing in each participating model, five passive tracers are included for predefined regional domains within the African continent. In addition, a stratospheric tracer is defined to diagnose the strength of intrusions from the stratosphere into the (upper) troposphere. Each passive tracer concentration is fixed below 850 hPa within the respective regional domain at an arbitrary concentration of 100 parts per trillion by volume (pptv) and given a fixed lifetime of 20 days. During the simulations, the passive tracers are

continually replenished for the relevant pressure limits every model time step. For the stratospheric tracer, the same procedure is used above the thermal tropopause in each respective model. The definitions of the latitudinal and longitudinal regions in which each of the passive tracers are initialized are given in Table 2.

**DIFFERENCES IN METEOROLOGY AND CONVECTIVE MIXING.** Here, we present direct comparisons of the resulting distributions of selected passive tracers between each of the participating models. For this purpose, we calculate and compare monthly means from the 3-hourly output fields for the 2D cross sections. The seasonality of the biomass burning seasons is governed by periods of extended dryness, meaning that the most intense burning activity occurs in northern Africa during the season December–February (DJF), whereas for southern Africa it occurs during the season September–November (SON; e.g., Giglio et al. 2006). Moreover, the movement of the intertropical convergence zone (ITCZ) throughout the year has the potential to make certain transport pathways between the hemispheres essentially “blocked.” Therefore, we show monthly means for both February and August to highlight the differences introduced between the NH winter and summer.

Figure 1 shows comparisons for February and August 2006 for the Sahel tracer between the participating models in order to highlight the differences in convective mixing. In general, the models driven by the ECMWF meteorological fields show similar tracer distributions for both months, although the southerly transport is more limited during August in all models as a consequence of the movement of the ITCZ. The MOCAGE model exhibits the strongest convective transport throughout the entire year. Moreover, TM4 shows the weakest convective activity during February, whereas p-TOMCAT shows the weakest convective activity during August, even though both adopt the scheme of Tietdke (1989). Comparing the tracer distribution between the different models supports the conclusions of previous studies (Josse et al. 2004), in that the Bechtold et al. (2001) parameterization exhibits stronger convective transport than Tietdke (1989), which leads to substantial differences for the upper troposphere. For the Emanuel (1991) scheme,

**TABLE 2. A definition of the passive tracers implemented for diagnosing atmospheric transport in the AMMA-MIP intercomparison. All tracers are defined between 20°W and 40°E and given a fixed lifetime of 20 days, except for the stratospheric tracer, which is defined globally above the local thermal tropopause.**

Name of passive tracer	Lat band	Type
Sahara	20°–30°N	Land
Sahel	10°–20°N	Land
Guinea	0°–10°N	Land
Southern Africa	0°–40°S	Land
South Atlantic	0°–40°S	Ocean
Stratosphere	Global	Lower stratosphere

the enhanced convection is not so obvious when comparing LMDz-INCA against p-TOMCAT.

Figure 2 shows the corresponding distribution for the southern African passive tracer. For this tracer, the actual source region occurs toward the east of the 2D transect used for calculating the cross sections. Thus, the tropospheric distribution of this tracer gives some indication as to the extent and efficiency of the advection of air away from the African continent toward the west for each season. It can be seen that, for NH winter, the maximal concentrations occur at higher altitudes than for the NH summer, possibly because of the change in the position of the ITCZ, where the tracer is lofted upward by convective mixing. Again, the highest tracer concentrations are exhibited by MOCAGE as a result of the strong convective transport that occurs over land. Another striking feature is that, for LMDz-INCA, the highest tracer concentrations are essentially isolated from the lower troposphere compared with, for example, p-TOMCAT, suggesting a different transport pathway

for both months. Moreover, transport north of the equator seems more efficient during the summer, where significant concentrations reach land (5°–10°N). For the same period, Mari et al. (2008) have used passive tracers in a Lagrangian parcel model to identify the efficient transport of biomass burning plumes out across the Atlantic Ocean in the Southern Hemispheric African easterly jet. Apart from a “break” phase that occurred during the first week of August, the transport of air containing significant chemical signatures of biomass burning activity remained persistent throughout the entire month. The contours in Fig. 2 show that the global CTMs also capture this movement of air for this period. Further analysis using the periods defined in Mari et al. (2008) indicate that this break phase is also captured in the CTMs (not shown).

**DIFFERENCES IN TRACE GAS DISTRIBUTIONS.** Figures 3 and 4 show the tropospheric distribution of CO and O<sub>3</sub> along the 2D transect for

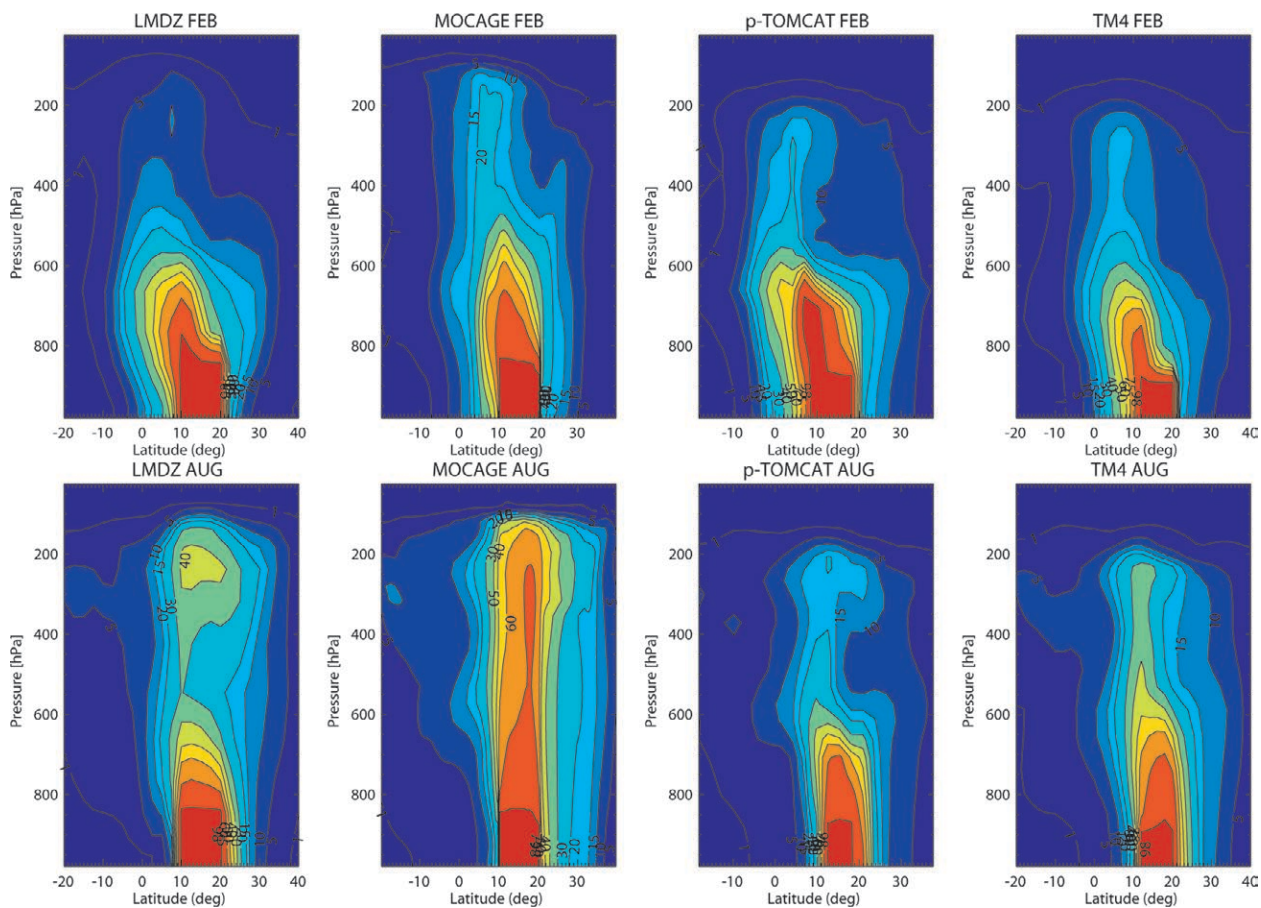


**FIG. 1.** Comparison of the monthly means of the tropospheric distribution of the Sahel passive tracer (10°–20°N) for (top) Feb and (bottom) Aug 2006, as calculated in each of the four participating CTMs within AMMA-MIP.

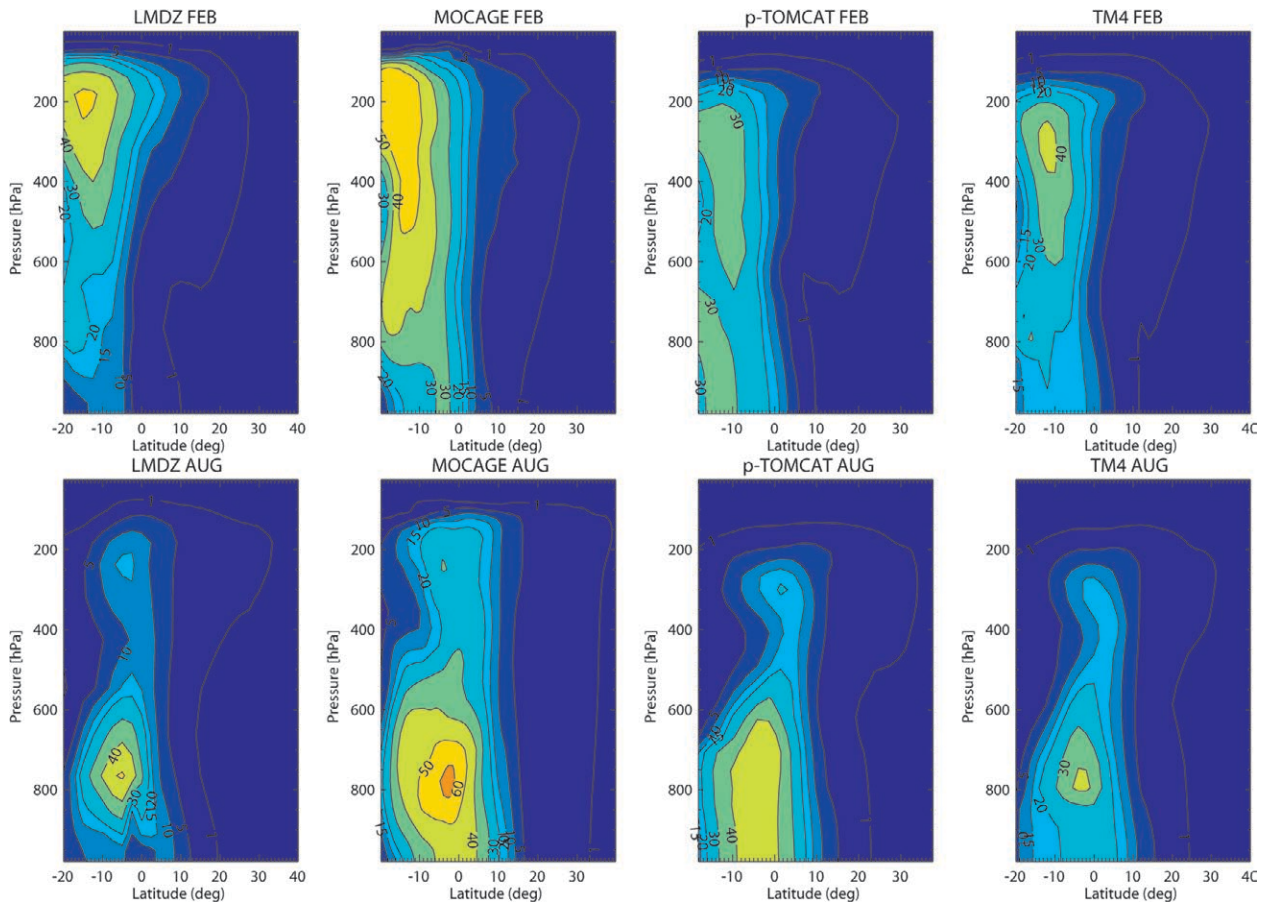


**FIG. 2.** Comparison of the monthly means of the tropospheric distribution of the southern Africa passive tracer (40°S–0°) for (top) Feb and (bottom) Aug 2006, as calculated in each of the four participating CTMs within the chemical component of AMMA-MIP. The 2D cross section does not pass directly over the source region; thus, the tracer distribution occurs as a result of advection from southern Africa over the southern Atlantic

February and August, respectively. Because  $O_3$  is not emitted directly, it is formed in situ as a typical air mass “ages” via photolytic and chemical reactions involving nitrogen oxides ( $NO_x$ ), hydrogen oxides ( $HO_x$ ), and nonmethane hydrocarbons (NMHCs). These diagrams clearly show that higher concentrations of both trace gas species occur during the summer, in line with the increased burning activity that occurs as defined in the L3JRCv2 emission dataset. Moreover, there is also a strong correlation with the maximum of the southern African passive tracer for August, indicating that the source of the high concentrations originates from this region.

Such concentrations are higher than those calculated using the corresponding GFEDv2 emission database (not shown), as would be expected, considering the substantial increase in emissions over the season JJA (not shown). For CO, which has a typical atmospheric lifetime of a few months, there are differences between the models in both

seasons. For instance, the pressure level at which the highest CO occurs during February varies between ~500 hPa (LMDz-INCA, p-TOMCAT) and ~800–900 hPa (MOCAGE, TM4). For August, although the distribution of CO is similar in all models, the maximum CO concentration varies by up to ~100 ppbv, indicating either faster transport or slower chemical destruction occurs between participating models. For  $O_3$ , TM4 exhibits the highest concentrations for both months of all the models, followed by MOCAGE, p-TOMCAT, and LMDz-INCA. This variability is principally due to differences in the chemical production efficiency of  $O_3$  and subsequent transport, as calculated by the various chemical mechanisms and transport parameterizations employed between models. For August, some similarity is observed in the distribution of the maximal CO and maximal  $O_3$ , indicating that the source region of reactive nitrogen precursors is the same as for CO. Comparisons against trace gas

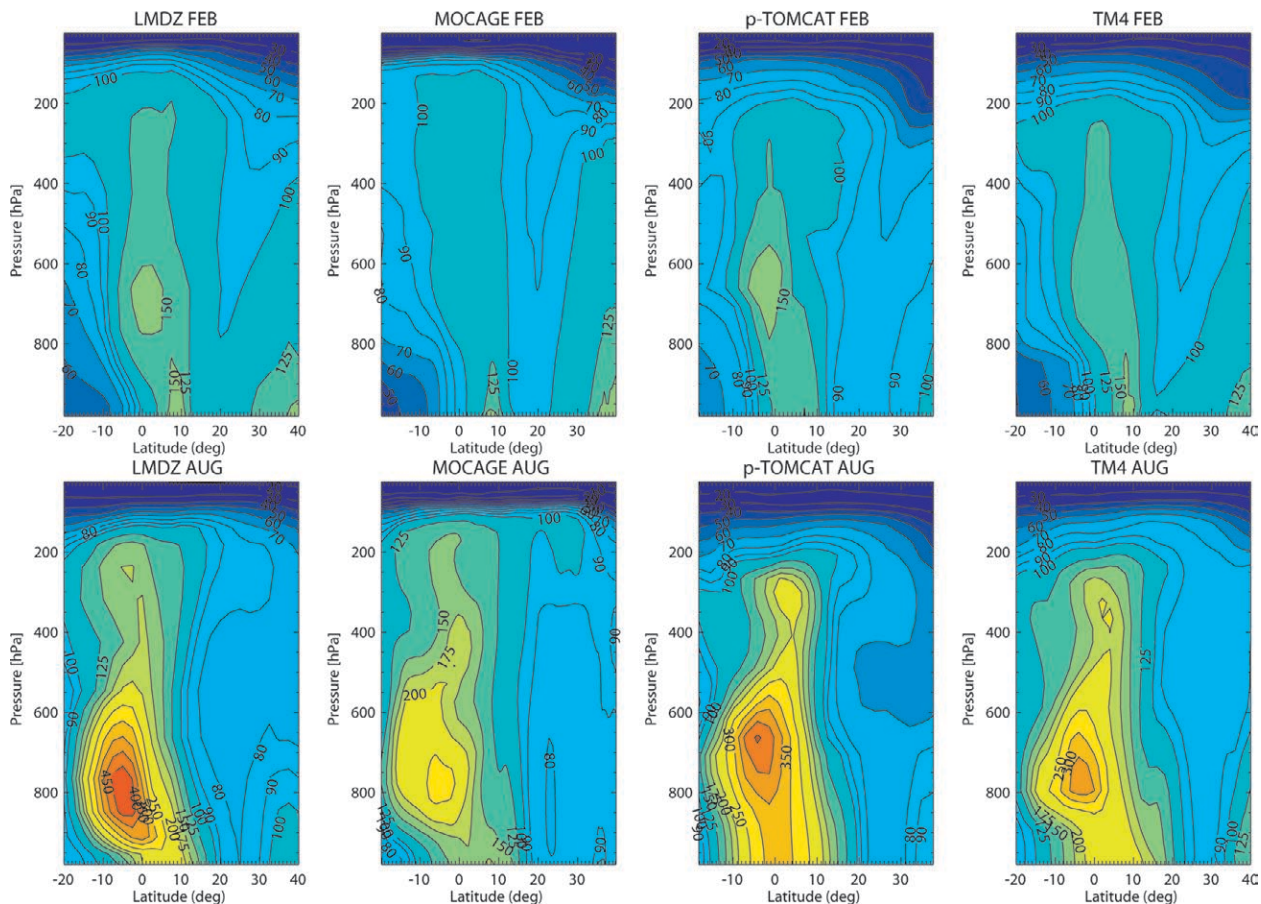


**FIG. 3.** Comparison of the monthly means for CO in ppbv for (top) Feb and (bottom) Aug 2006, as calculated in each of the four global CTMs within AMMA-MIP. It can be seen that higher concentrations occur during Aug, which correlates with maximal emissions in central Africa because of intensive biomass burning.

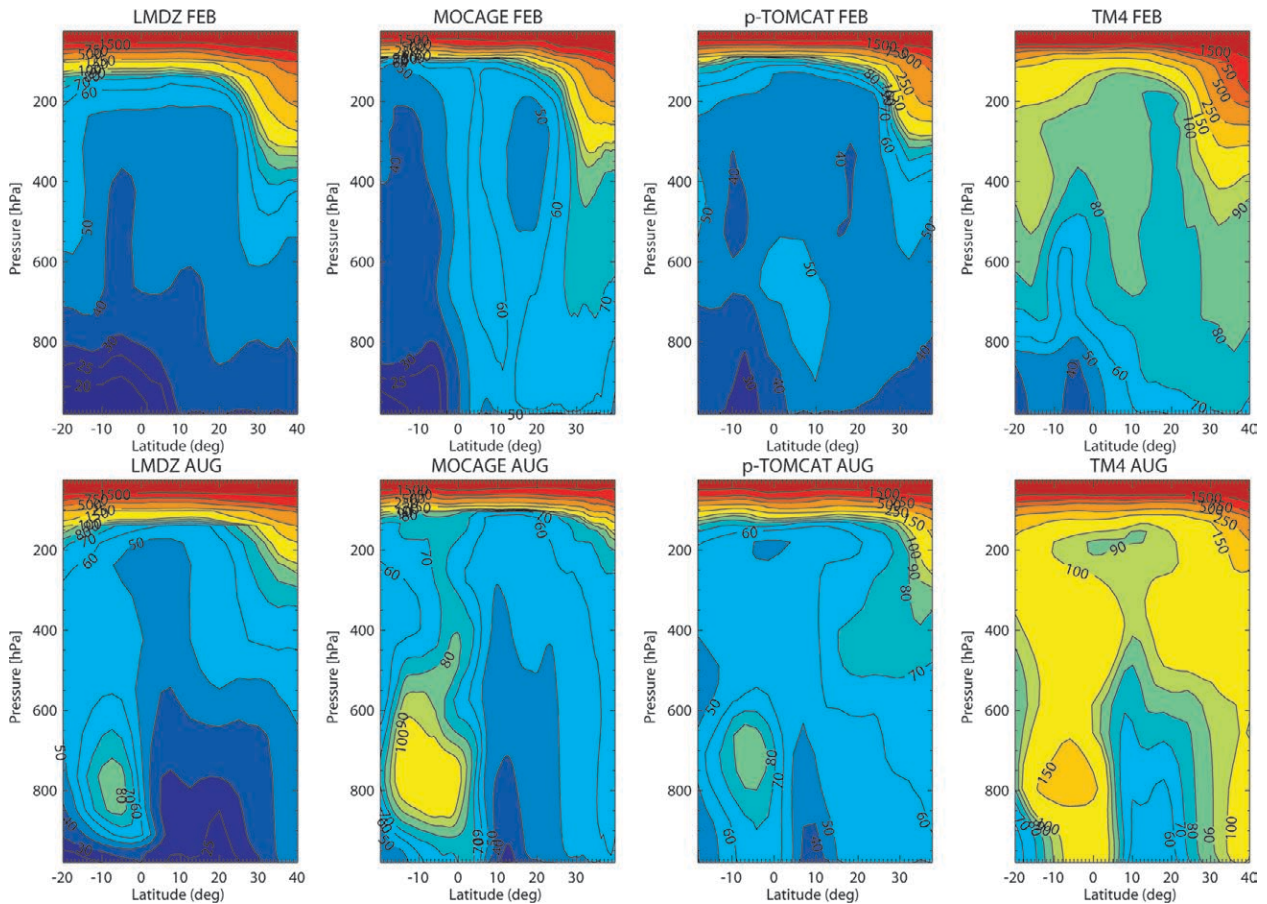
distributions calculated using the GFEDv2 inventory (not shown) indicate that the sequestration of reactive nitrogen into more stable reservoir species [e.g., peroxyacetyl nitrate (PAN)] increases in some models, allowing more O<sub>3</sub> production away from the main source region when applying the L3JRCv2 emission dataset.

Figure 5 shows the corresponding distributions for the stratospheric tracer. The differences between models are relatively large, where TM4 exhibits the strongest STE for the upper troposphere and MOCAGE exhibits the most influence at the surface in the NH. There is some similarity between the tropospheric distribution of the stratospheric tracer and the distribution in tropospheric O<sub>3</sub>, especially in the NH for MOCAGE. However, using a chemically active stratospheric O<sub>3</sub> tracer (not shown), the stratospheric contribution is at maximum ~10% in TM4 below 200 hPa between 10°S and 10°N, which has the highest O<sub>3</sub> concentrations of all models as well as the strongest STE in the upper troposphere.

For latitudes of >20°N the contribution approximately doubles. Moreover, comparing differences between simulations using the GFEDv2 biomass burning dataset show that ~50% of the O<sub>3</sub> maximum is a direct consequence of the increase in monthly emissions in the L3JRCv2 dataset. For the other CTMs, the individual contributions are somewhat dependent on the chemical lifetime of O<sub>3</sub> in the particular model, but it is expected that the contribution is of a similar magnitude, considering the weaker downwelling shown in Fig. 5.

### COMPARISONS WITH OBSERVATIONS.

Figure 6 shows a comparison of the seasonal composite for JJA of ozonesondes launched from Cotonou (6.2°N, 2.2°E) on the Nigerian coast (Thouret et al. 2009) and the corresponding colocated output from the participating models. For the calculation of the model profiles, only those profiles output on the corresponding launch dates of the measurements are used. It can be clearly seen that MOCAGE has the

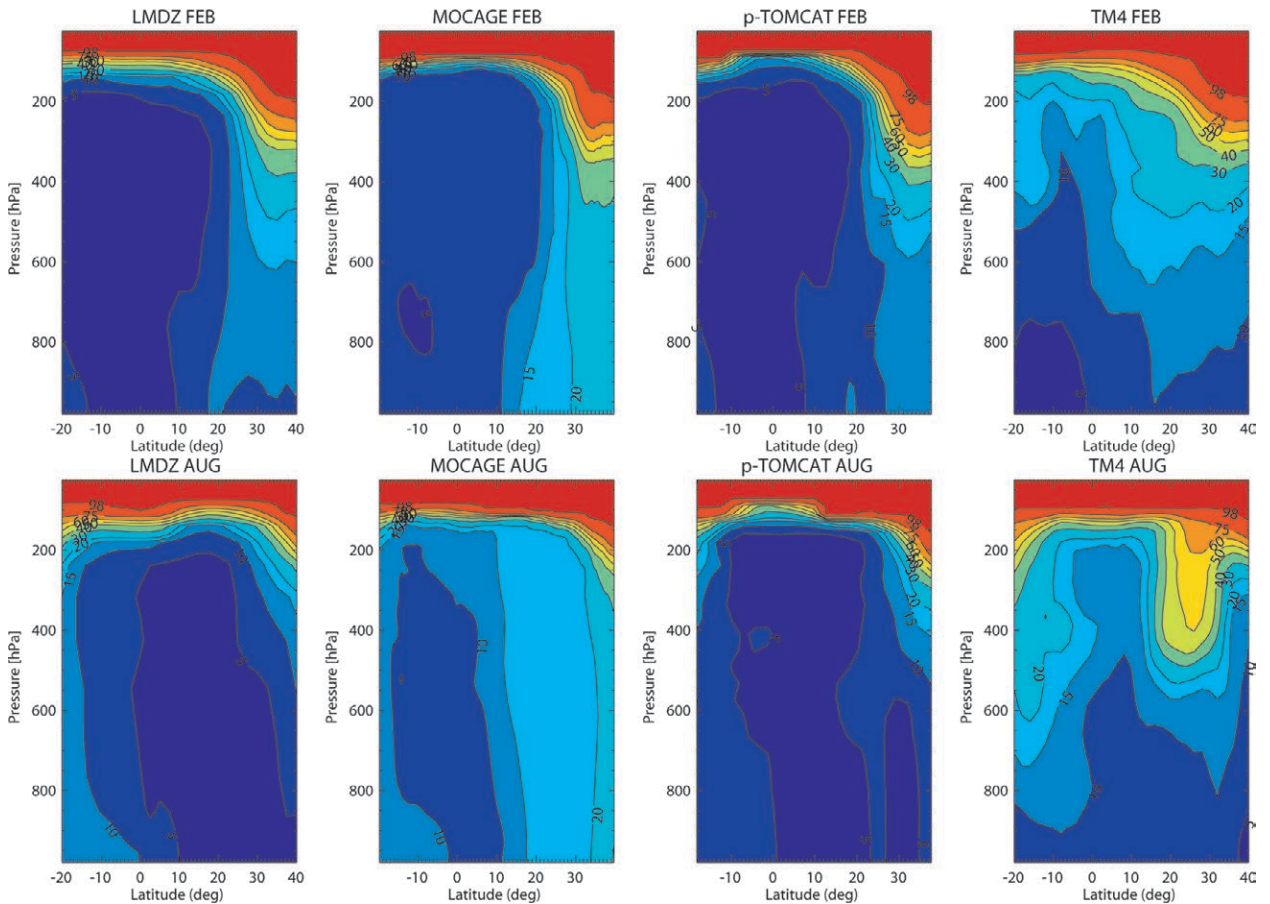


**FIG. 4.** Comparison of the monthly means for  $O_3$  in ppbv for Feb and Aug 2006, respectively, as calculated in each of the four global CTMs within AMMA-MIP. The higher concentrations calculated in Aug are the result of the increased emission, chemical sequestration, and transport of  $NO_2$ .

highest surface ozone values (by nearly 200% for this location), whereas both LMDz-INCA and TM4 show better agreement in the lower troposphere, although they still overestimate. A contributing factor could be that the loss of  $O_3$  via dry deposition is not described adequately in the models, especially the uptake by vegetation (e.g., Williams et al. 2009). For the upper troposphere, p-TOMCAT shows the best agreement, although a difference of ~25% still occurs between 200 and 400 hPa. It is also interesting to note that the standard deviation for both LMDz-INCA and p-TOMCAT is much smaller than that exhibited by the other models, suggesting that variability in tropospheric ozone is not as enhanced. Examining the profiles from individual ozonesondes shows there is large variability for this station, where an “extreme” event was observed on 14 August (Thouret et al. 2009), which has recently been attributed to southern biomass burning (Real et al. 2010). Thus, it appears that all models have difficulty in capturing the correct transport into the region, regardless of the

meteorology adopted to drive the model. Moreover, the profiles of TM4 and LMDz-INCA are remarkably similar, considering the difference in vertical resolution and the combination of parameterizations used for the transport of emissions. Similar comparisons for ozone radio soundings taken from Nariobi, Kenya (1.3°S, 36.8°E), do not show such a deviation between the models and measurement seasonal means below 400 hPa (not shown), despite a lower sampling frequency, indicating that there is more variation in the transport pathways at Cotonou, which introduces large seasonal variability.

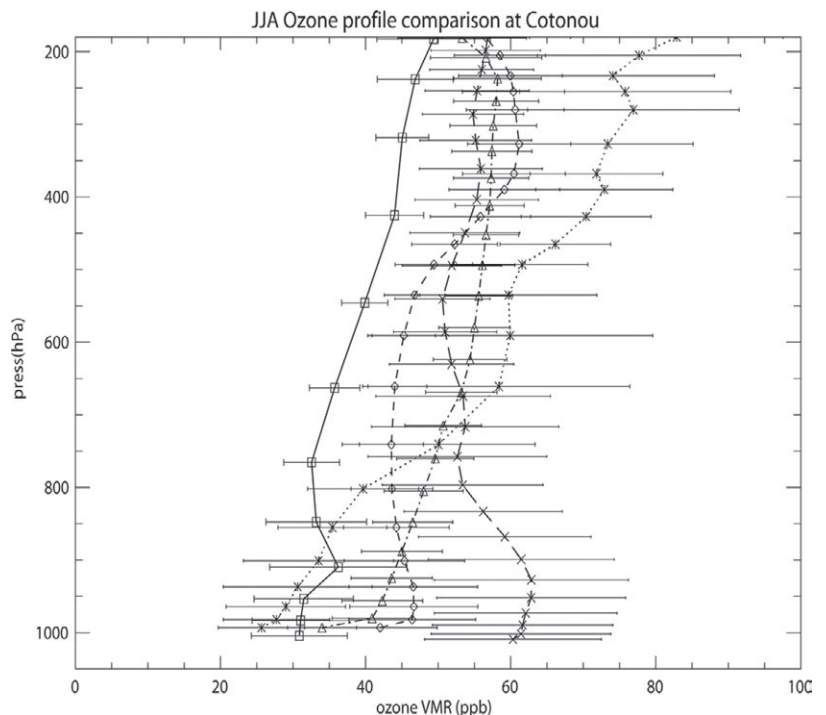
Another factor that influences the comparisons is the performance of the different chemical schemes that are employed. For instance, Prather (2009) recently has shown that accounting for the photolysis of  $O_2$  is important for tropical tropospheric ozone in the upper troposphere down to 10-km altitude. In the comparison shown in Fig. 6, such improvements are not so obvious where, for example, LMDz-INCA includes this photolysis rate but TM4 does not.



**FIG. 5.** Comparison of the monthly means of the tropospheric distribution of the stratospheric passive tracer initialized above the thermal tropopause for (top) Feb and (bottom) Aug 2006, as calculated in each of the four participating CTMs within AMMA-MIP.

Another difference is that not all the NMHC emissions are included in all the models because of the number of chemical species included in each scheme. When comparing the spread in the models shown in Fig. 4, it can be seen that at this latitude ( $6.2^{\circ}\text{N}$ ) the differences between the  $\text{O}_3$  values calculated between the models are much less than when considering

**FIG. 6.** A comparison of ozonesonde measurements taken at Cotonou ( $6.2^{\circ}\text{N}$ ,  $2.2^{\circ}\text{E}$ ) with output from model simulations for JJA in 2006: observations (asterisks), LMDz-INCA (squares), TM4 (diamonds), MOCAGE (Xs) and p-TOMCAT (triangles). The error bars represent  $1\text{-}\sigma$  standard deviations for each of the respective datasets.



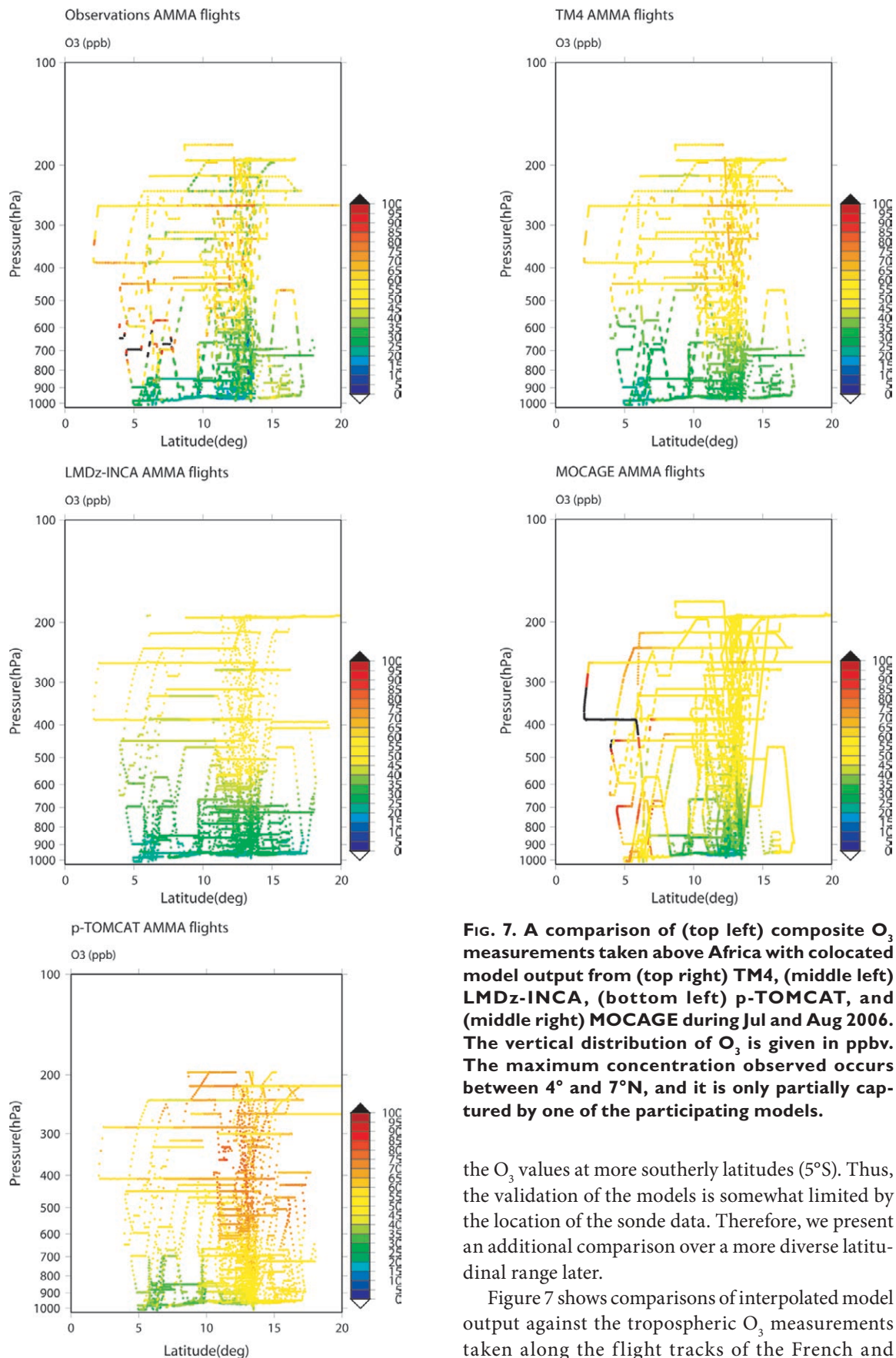


**FIG. 7.** A comparison of (top left) composite  $O_3$  measurements taken above Africa with colocated model output from (top right) TM4, (middle left) LMDz-INCA, (bottom left) p-TOMCAT, and (middle right) MOCAGE during Jul and Aug 2006. The vertical distribution of  $O_3$  is given in ppbv. The maximum concentration observed occurs between 4° and 7°N, and it is only partially captured by one of the participating models.

the  $O_3$  values at more southerly latitudes (5°S). Thus, the validation of the models is somewhat limited by the location of the sonde data. Therefore, we present an additional comparison over a more diverse latitudinal range later.

Figure 7 shows comparisons of interpolated model output against the tropospheric  $O_3$  measurements taken along the flight tracks of the French and

German Falcon and the British BAe146 for the AMMA measurement campaign as shown in previous work (with the exception of the M55-Geophysica measurements; Janicot et al. 2008). The maximal O<sub>3</sub> concentrations occur in the middle troposphere between 4° and 7°N, most likely because of emissions from biomass burning (e.g., Thouret et al. 2009; Real et al. 2010). Table 3 provides

**TABLE 3. Pearson's correlation coefficients between the colocated CTM output and measurements made by the French and German Falcon and the British BAe146 for the AMMA measurement campaign. Individual correlation coefficients are given for the lower (800 hPa and below), middle (800–500 hPa), and upper (500 hPa upward), as well as the cumulative value, for each participating model.**

Model	All	Lower (>800 hPa)	Middle (800–500 hPa)	Upper (<500 hPa)
LMDz-INCA	0.46 ± 0.03	0.19 ± 0.02	0.08 ± 0.03	-0.14 ± 0.05
MOCAGE	0.60 ± 0.03	0.35 ± 0.14	0.76 ± 0.03	0.29 ± 0.06
TM4	0.00 ± 0.03	-0.25 ± 0.16	-0.17 ± 0.05	-0.36 ± 0.04
p-TOMCAT	0.48 ± 0.03	0.66 ± 0.08	-0.43 ± 0.03	0.65 ± 0.04

the Pearson correlation coefficients between measurements and the model results, where values are given for the lower, middle, and upper troposphere. The correlation is performed using values obtained by averaging all points from either the measurements or individual models in 0.5° latitude bins and 50-hPa pressure bins. These results show that there are large differences between the performance of the different models, with TM4 (MOCAGE) having the worst (best) correlation coefficient overall. In fact, TM4 generally shows a low anticorrelation with the height-segregated measurements, whereas MOCAGE shows a medium correlation (with the correlation in the middle troposphere being quite high). Interestingly, these two models are the only ones to exhibit O<sub>3</sub> concentrations around ~100 ppbv along the flight tracks, although only MOCAGE captures the correct latitudinal distribution but at a higher altitude. For p-TOMCAT, there is a medium correlation in the lower and upper troposphere, with an anticorrelation in the middle troposphere. LMDz-INCA generally shows a low correlation throughout the troposphere. This is surprising, considering that LMDz-INCA generally shows low values in the lower troposphere and high values in the middle to upper troposphere, as with the measurements. Further analysis using the different transport periods identified in Mari et al. (2008; not shown) reveals that high values in both CO and O<sub>3</sub> correlate with the southern African tracer over the southern Atlantic Ocean. However, Fig. 6 has shown that there is generally an underestimation in the tropospheric ozone profile simulated in these global CTMs, which also influences the atmospheric composition above the AMMA measurement region.

Other comparisons with the CO and O<sub>3</sub> profiles measured at Windhoek, Namibia (22.5°S, 17.5°E), taken as part of the MOZAIC program reveal that simulations using the L3JRCv2 inventory substantially

overestimate surface O<sub>3</sub> in southern Africa compared to simulations using the GFEDv2 inventory (not shown). The high concentrations of both trace gases measured during the AMMA campaign are thought to be due to the transport of polluted air containing signatures resulting from biomass burning in southern Africa (Real et al. 2010). The fact that most of the models cannot capture such events and the fact that the maximal concentrations occur between 0° and 5°S (cf. Figs. 3, 4) indicate that the continental transport within Africa is not optimal. Additional forward trajectory calculations using 1° × 1° ECMWF meteorological data in the Royal Netherlands Meteorological Institute (KNMI) trajectory model (TRAJKS; Scheele et al. 1996) started between 1.5 and 3 km above the surface between 10° and 15°S (25°–30°E) reveal that the air flows predominantly toward the northwest and does not impinge the location at which maximal O<sub>3</sub> concentrations were measured by the AMMA flight measurements and ozone sondes. Back trajectories performed to identify the origin of air containing the extreme O<sub>3</sub> concentrations on 14 August indicate that air circles around the measurement site for ~5 days preceding the measurement, before heading west rather than south. This could be associated with blocking, identified as the break period in transport into the region between 3 and 8 August (Mari et al. 2008). It could also be due to a strong local emission source that is missing from the inventories, although similar results occur when adopting the GFEDv2 inventories (not shown). Further investigations are underway to elucidate what is the most probable cause of this deficiency toward capturing the seasonal variation near equatorial Africa.

**CONCLUSIONS AND OUTLOOK.** Here we have briefly shown a sample of the results obtained during the chemistry-transport modeling compo-

ment of the AMMA-MIP exercise, where our focus has been to exploit the 2D cross-sectional data with the aim of representing the “zonality” of the West African monsoon. These simulations are the first time the recently developed J3LRCv2 emission dataset has been used for CTM modeling of the African region, albeit as monthly aggregates. The results of combining different parameterizations to simulate the transport of chemical trace gas species are significant differences in convective uplifting and subsequent transport of air masses westward out of southern Africa. In general, the models show maximal concentrations in both CO and O<sub>3</sub> around 5°S and tend to miss the high concentrations of O<sub>3</sub> observed above 5°N in the middle of August. This could be due to either missing transport processes or to a strong local emission source, which is missing in the inventory. Moreover, the participating models generally show surface ozone that is too high but underpredicting ozone in the free troposphere when compared to sonde measurements made on the West African coast, possibly because of inadequacies in the dry deposition fluxes and/or chemical mechanisms employed.

**ACKNOWLEDGEMENTS.** The authors acknowledge the EU integrated project African Monsoon Multidisciplinary Analysis (AMMA) for the support network and funding. Based on a French initiative, AMMA was built by an international scientific group and is currently funded by a large number of agencies, especially from France, the United Kingdom, the United States, and Africa. It has been the beneficiary of a major financial contribution from the European Community Sixth Framework Research Programme. Detailed information on scientific coordination and funding is available on the AMMA International Web site ([www.amma-international.org](http://www.amma-international.org)). Additionally, XY acknowledges AMMA-UK and the NCAS, and KL/IB acknowledge financial support from the AMMA-France project. The authors are grateful to Hans Schlager (DLR), Gerard Ancellet (Service d’Aeronomie), and the Facility for Airborne Atmospheric Measurements (FAAM) for permission to use the measurements taken during the AMMA measurement campaign.

## REFERENCES

Ancellet, G., J. Leclair de Bellevue, C. Mari, P. Nédélec, A. Kukai, A. Borbon, and P. Perros, 2009: Effects of regional-scale and convective transports on tropospheric ozone chemistry revealed by aircraft observations during the wet season of the AMMA campaign. *Atmos. Chem. Phys.*, **9**, 383–411.

Barret, B., and Coauthors, 2010: Impact of West African monsoon convective transport and lightning NO<sub>x</sub> production upon tropical composition of the upper troposphere. *Atmos. Chem. Phys.*, in press.

Bechtold, P., E. Bazile, F. Guichard, P. Mascart, and E. Richard, 2001: A mass-flux convection scheme for regional and global models. *Quart. J. Roy. Meteor. Soc.*, **127**, 869–886.

Bian, H., M. Chen, S. R. Kawa, B. Duncan, A. Arellano, and P. Kasibhatla, 2007: Sensitivity of global CO simulations to uncertainties in biomass burning sources. *J. Geophys. Res.*, **112**, D23308, doi:10.1029/2006JD008376.

Bönisch, H., P. Hoor, Ch. Gurk, W. Feng, M. Chipperfield, A. Engel, and B. Bregman, 2008: Model evaluation of CO<sub>2</sub> and SF<sub>6</sub> in the extratropical UT/LS region. *J. Geophys. Res.*, **113**, D06101, doi:10.1029/2007JD008829.

Carver, G. D., P. D. Brown, and O. Wild, 1997: The ASAD atmospheric chemistry integration package and chemical reaction database. *Comput. Phys. Comm.*, **105**, 197–215.

Duncan, B. N., J. J. West, Y. Yoshida, A. M. Fiore, and J. R. Ziemke, 2008: The influence of European pollution on ozone in the Near East and northern Africa. *Atmos. Chem. Phys.*, **8**, 2267–2283.

Emanuel, K. A., 1991: A scheme for representing cumulus convection in large-scale models. *J. Atmos. Sci.*, **48**, 2313–2335.

Folberth, G. A., D. A. Hauglustaine, J. Lathière, and F. Brocheton, 2006: Interactive chemistry in the Laboratoire de Météorologie Dynamique general circulation model: Model description and impact analysis of biogenic hydrocarbons on tropospheric chemistry. *Atmos. Chem. Phys.*, **6**, 2273–2319.

Fortuin, P. F. J., and H. Kelder, 1998: An ozone climatology based on ozonesonde and satellite measurements. *J. Geophys. Res.*, **103**, 31 709–31 734.

Giglio, L., G. R. van der Werf, J. T. Randerson, G. J. Collatz, and P. S. Kasidhatla, 2006: Global estimation of burned area using MODIS active fire observations. *Atmos. Chem. Phys.*, **6**, 957–974.

Holtslag, A. A. M., and B. A. Boville, 1993: Local versus nonlocal boundary-layer diffusion in a global climate model. *J. Climate*, **6**, 1825–1842.

Hourdin, F., and Coauthors, 2006: The LMDz4 general circulation model: Climate performance and sensitivity to parameterized physics with emphasis on tropical convection. *Climate Dyn.*, **27** (7–8), 787–813, doi:10.1007/s00382-006-0158-0.

—, and —, 2010: AMMA-Model Intercomparison Project. *Bull. Amer. Meteor. Soc.*, **91**, 95–104.

- Houweling, S., F. J. Dentener and J. Lelieveld, 1998: The impact of non-methane hydrocarbon compounds on tropospheric photochemistry. *J. Geophys. Res.*, **103**, 10 673–10 696.
- Ito, A., and J. E. Penner, 2004: Global estimates of biomass burning emissions based on satellite imagery for the year 2000. *J. Geophys. Res.*, **109**, D14S05, doi:10.1029/2003JD004423.
- Jain, A. K., 2007: Global estimation of CO emissions using three sets of satellite data for burned area. *Atmos. Environ.*, **41**, 6931–6940.
- Janicot, S., and Coauthors, 2008: Large-scale overview of the summer monsoon over West Africa during the AMMA field experiment in 2006. *Ann. Geophys.*, **26**, 2569–2595.
- Josse, B., P. Simon, and V.-H. Peuch, 2004: Radon global simulations with the multiscale chemistry transport model MOCAGE. *Tellus*, **56B**, 339–356.
- Krol, M. C., and M. van Weele, 1997: Implications of variations in photodissociation rates for global tropospheric chemistry. *Atmos. Environ.*, **31**, 1257–1273.
- Landgraf, J., and P. J. Crutzen, 1998: An efficient method for online calculations of photolysis and heating rates. *J. Atmos. Sci.*, **55**, 863–878.
- Law, K. S., and J. A. Pyle, 1993: Modeling trace gas budgets in the troposphere: 1. O<sub>3</sub> and odd nitrogen. *J. Geophys. Res.*, **98**, 18 377–18 400.
- , and E. Nisbet, 1996: Sensitivity of the methane growth rate to changes in methane emissions from natural gas and coal. *J. Geophys. Res.*, **101**, 14 387–14 397.
- Lefèvre, F., G. P. Brasseur, I. Folkins, A. K. Smith, and P. Simon, 1994: Chemistry of the 1991–1992 stratospheric winter: Three-dimensional model simulations. *J. Geophys. Res.*, **99**, 8183–8195.
- Lioussé, C., and Coauthors, 2004: Deriving global quantitative estimates for spatial and temporal distributions of biomass burning emissions. *Emissions of Atmospheric Trace Compounds*, C. Granier, P. Artaxo, and C. E. Reeves, Eds., Kluwer Academic, 71–113.
- , and Coauthors, 2010: Western African aerosols modelling with biomass burning emission inventories in the frame of the AMMA-IDAF program. *Atmos. Chem. Phys.*, in press.
- Louis, J. F., 1979: A parametric model of vertical eddy fluxes in the atmosphere. *Bound.-Layer Meteor.*, **17**, 182–202.
- Madronich, S., and S. Flocke, 1998: The role of solar radiation in atmospheric chemistry. *Handbook of Environmental Chemistry*, P. Boule, Ed., Springer-Verlag, 1–26.
- Mari, C. H., G. Cailley, L. Corre, M. Saunois, J. L. Attié, V. Thouret, and A. Stohl, 2008: Tracing biomass burning plumes from the Southern Hemisphere during the AMMA 2006 wet season experiment. *Atmos. Chem. Phys.*, **8**, 3951–3961.
- Michel, C., C. Lioussé, J.-M. Grégoire, K. Tansey, G. R. Carmichael, and J.-H. Woo, 2005: Biomass burning emission inventory from burnt area data given by the SPOT-VEGETATION system in the frame of TRACE-P and ACE-Asia campaigns. *J. Geophys. Res.*, **110**, D09304, doi:10.1029/2004JD005461.
- Prather, M. J., 1986: Numerical advection by conservation of second-order moments. *J. Geophys. Res.*, **91**, 6671–6681.
- , 2009: Tropospheric O<sub>3</sub> from the photolysis of O<sub>2</sub>. *Geophys. Res. Lett.*, **36**, L03811, doi:10.1029/2008GL036851.
- Rasch, P. J., and D. L. Williamson, 1990: On shape-preserving interpolation and semi-Lagrangian transport. *SIAM J. Sci. Stat. Comput.*, **11**, 656–687.
- Real, E., and Coauthors, 2010: Cross-hemispheric transport of central African biomass burning pollutants: Implications for downwind ozone production. *Atmos. Chem. Phys. Discuss.*, **10**, 3027–3046.
- Reeves, C. E., and Coauthors, 2010: Chemical and aerosol characterisation of the troposphere over West Africa during the monsoon period as part of AMMA. *Atmos. Chem. Phys., Discuss.*, **10**, 7115–7183.
- Russell, G., and J. Lerner, 1981: A new finite-differencing scheme for tracer transport equation. *J. Appl. Meteor.*, **20**, 1483–1498.
- Sauvage, B., V. Thouret, J.-P. Cammas, F. Gheusi, G. Athier, and P. Nedelec, 2005: Tropospheric ozone over Equatorial Africa: Regional aspects from the MOZAIK data. *Atmos. Chem. Phys.*, **5**, 311–335.
- , and Coauthors, 2007a: Medium-range mid-tropospheric transport of ozone and precursors over Africa: Two numerical case studies in dry and wet seasons. *Atmos. Chem. Phys.*, **7**, 5357–5370.
- , and Coauthors, 2007b: Remote sensed and in situ constraints on processes affecting tropical tropospheric ozone. *Atmos. Chem. Phys.*, **7**, 815–838.
- Scheele, M. P., P. C. Siegmund, and P. F. J. van Velthoven, 1996: Sensitivity of trajectories to data resolution and its dependence on the starting point: In or outside a tropopause fold. *Meteor. Appl.*, **3**, 267–273.
- Simon, M., S. Plummer, F. Fierens, J. J. Hoelzemann, and O. Arino, 2004: Burnt area detection at global scale using ATSR-2: The GLOBSCAR products and their quantification. *J. Geophys. Res.*, **109**, D14S03, doi:10.1029/2003JD003622.

- Stockwell, W. R., F. Kirchner, M. Kuhn, and S. Seefeld, 1997: A new mechanism for regional atmospheric modeling. *J. Geophys. Res.*, **102**, 25 847–25 879.
- Teyssède, H., and Coauthors, 2007: A new tropospheric and stratospheric Chemistry and Transport Model MOCAGE-Climat for multi-year studies: Evaluation of the present-day climatology and sensitivity to surface processes. *Atmos. Chem. Phys.*, **7**, 5815–5860.
- Thouret, V., and Coauthors, 2009: An overview of two years of ozone radio soundings over Cotonou as part of AMMA. *Atmos. Chem. Phys.*, **9**, 6157–6174.
- Tiedtke, M., 1989: A comprehensive mass flux scheme for cumulus parameterization in large-scale models. *Mon. Wea. Rev.*, **117**, 1779–1800.
- van der Werf, G. R., J. T. Randerson, L. Giglio, G. J. Collatz, P. S. Kasibhatla, and A. F. Arellano Jr., 2006: Interannual variability in global biomass burning emissions from 1997 to 2004. *Atmos. Chem. Phys.*, **6**, 3423–3441.
- Van Leer, B., 1977: Towards the ultimate conservative difference scheme. Part IV: A new approach to numerical convection. *J. Comput. Phys.*, **23**, 276–299.
- Wang, K.-Y., J. A. Pyle, M. G. Sanderson, and C. Bridgeman, 1999: Implementation of a convective atmospheric boundary layer scheme in a tropospheric chemistry transport model. *J. Geophys. Res.*, **104**, 23 729–23 745.
- Williams, J. E., M. P. Scheele, P. F. J. van Velthoven, J.-P. Cammas, V. Thouret, C. Galy-Lacaux, and A. Volz-Thomas, 2009: The influence of biogenic emissions from Africa on tropical tropospheric ozone. *Atmos. Chem. Phys.*, **9**, 5729–5749.
- Williamson, D. L., and P. J. Rasch, 1989: Two-dimensional semi-Lagrangian transport with shape-preserving interpolation. *Mon. Wea. Rev.*, **117**, 102–129.
- Yang, X., R. A. Cox, N. J. Warwick, J. A. Pyle, G. D. Carver, F. M. O'Connor, and N. H. Savage, 2005: Tropospheric bromine chemistry and its impacts on ozone: A model study. *J. Geophys. Res.*, **110**, D23311, doi:10.1029/2005JD006244.